Ceramics International 45 (2019) 13187–13192

Contents lists available at ScienceDirect

Ceramics International

journal homepage: www.elsevier.com/locate/ceramint

# Reversible redox behavior of $Fe_2O_3/TiO_2$ composites in the gaseous photodegradation process

Xueping Dai[a,b,1], Guanhong Lu[a,1], Yidan Hu[a], Xiaofeng Xie[a,*], Xiao Wang[a], Jing Sun[a,**]

[a] Shanghai Institute of Ceramics, Chinese Academy of Sciences, 1295 Dingxi Road, Shanghai, 200050, China
[b] University of Chinese Academy of Sciences, 19 (A) Yuquan Road, Beijing, 100049, China

ARTICLE INFO

*Keywords:*
Photocatalysis
Redox behavior
$Fe_2O_3/TiO_2$
VOCs removal
Regeneration

ABSTRACT

The use of photocatalytic technology in VOCs pollutants removal has caused great attention. $Fe_2O_3$ possesses some unique advantages among diverse visible-light driven photocatalysts due to its narrow bandgap, abundant reserves and favorable biosafety. In this work, $Fe_2O_3/TiO_2$ composites was fabricated by a facile impregnation method and their photocatalytic performance towards acetaldehyde and o-xylene was detected. TEM, EDS, photoluminescence spectra and UV-Vis were used to characterize the morphology and properties of the $Fe_2O_3/TiO_2$ composites. It was proved that the photocatalytic ability of $TiO_2$ was greatly improved by coupling with $Fe_2O_3$. Interestingly, the $Fe_2O_3/TiO_2$ composites showed deactivation in the degradation of acetaldehyde while no such phenomenon in the o-xylene case. The reason could be that $Fe^{3+}$ accepted the photo-induced electrons of $TiO_2$ and was reduced to $Fe^{2+}$, which can easily combine with the intermediate product of acetaldehyde and generated $Fe(CH_3COO)_2$. Moreover, the deactivated photocatalyst can be regenerated by heat treatment, since $Fe(CH_3COO)_2$ can be decomposed into $Fe_2O_3$ in air. ESR was further used to demonstrate this mechanism. This work reveals the coupled redox reactions in the photocatalytic process, which is benefit for the design of new photocatalysts.

## 1. Introduction

Volatile organic compounds (VOCs), as common pollutants in the air, have attracted great attention recently, mainly because of their potential to cause some health problems [1–6]. Among the air purification methods, photocatalytic oxidation process has been widely studied about its applications due to its non-toxic, broad-spectrum and longevity of service [7–10]. $TiO_2$ is generally used as a semiconductor photocatalyst because it is physicochemical stable, non-toxic, low-cost and with excellent photocatalytic activity under ultraviolet irradiation [11]. However, $TiO_2$ has low light response range and high photoelectron hole recombination rate, which limits its application in photocatalysis [12–17]. Many studies have focused on solving the two disadvantages of $TiO_2$, such as constructing heterostructure with narrow band gap semiconductor [18–21]. $Fe_2O_3$ is currently considered as one of the most promising semiconductor materials for photocatalytic process due to a series of desirable properties, including adequate absorption from visible light region in solar spectrum (bandgap is about 2.3eV), excellent stability in the air, and earth-abundant [22–24].

Therefore, $Fe_2O_3$ modified $TiO_2$ heterojunction composites have been widely reported. For instance, Alireza Banisharif et al. synthesized $Fe_2O_3$-$TiO_2$ by an ultrasonic-assisted coprecipitation method and used it to degrade 500 ppm trichloroethylene (TCE) in air [25]. Amarjargal et al. prepared $TiO_2$ decorated α-$Fe_2O_3$ microflowers heterostructure, which obtained much better photocatalytic efficiency about 92% towards Methyl blue (MB) degradation after 80 min under visible light irradiation [26]. Hua Tang et al. synthesized the novel α-$Fe_2O_3/TiO_2$ composite hollow spheres, which showed an excellent performance in the photocatalytic degradation of Rhodamine B (RhB) in aqueous solution under visible light [27]. Although $Fe_2O_3$ modification has been widely demonstrated to effectively improve visible light response of catalysts, the photocatalytic process is still unclear. According to some reports, the mechanism of promoting the separation of photo-induced electron hole pairs is mainly due to that $Fe^{3+}$ was reduced to $Fe^{2+}$ by trapping electrons. However, this hypothesis is devoid of direct experimental evidence. Electron spin resonance (ESR) is a magnetic resonance technique that generates magnetic moments of unpaired electrons, which can be used to qualitatively and quantitatively detect the

* Corresponding author.
** Corresponding author.
*E-mail addresses:* xxfshcn@163.com (X. Xie), jingsun@mail.sic.ac.cn (J. Sun).
[1] Xueping Dai and Guanhong Lu contributed equally to this work.

https://doi.org/10.1016/j.ceramint.2019.03.255
Received 23 March 2019; Received in revised form 31 March 2019; Accepted 31 March 2019
Available online 03 April 2019

unpaired electrons in atoms or molecules and explore the structural characteristics. ESR has been widely used to explore the processes of charge transfer in the photocatalytic reaction [28,29]. Peng et al. used ESR signals at ultra-low-temperature (1.8 K) to study $TiO_2/Fe_2O_3$ nanocomposites and observed the generation of $Ti^{3+}$ after illumination [30,31]. However, since the paramagnetism of $Fe^{3+}$ has an intervention to the signal of ESR, few work try to detect the signal of ESR after photodegradation process, which may directly probe the generation of $Fe^{2+}$.

In this work, $TiO_2/Fe_2O_3$ composites with different Ti/Fe molar ratios were prepared and their photocatalytic properties towards different polluted gases (acetaldehyde and o-xylene) were tested under 260 w fluorescent lamps. Interestingly, the oxidation product of acetaldehyde can combine with $Fe^{2+}$ and cause the deactivation of the photocatalyst while there was no such phenomenon in the case of o-xylene degradation. The supposition of $Fe^{3+}$ reducing to $Fe^{2+}$ by trapping electrons preliminarily confirmed by the change of ESR signal. This result provides a new idea for characterizing the mechanism that variable valence metal ions promote the separation of electrons and holes in photocatalytic process.

## 2. Experimental section

### 2.1. Materials preparation

All the chemicals are commercially available and used as received without any further purification, including P25 bought from Evonik Industries AG, Iron nitrate nonahydrate ($Fe(NO_3)_3{\cdot}9H_2O$, AR,65–68%, Sinapharm Chemical Reagent Co., Ltd) and ethanol ($C_2H_6O$, AR, 99.7%, Zhenxing No.1 Chemical Plant).

The $Fe_2O_3$-$TiO_2$ composites were prepared by a simple impregnation and calcination method. Typically, 2.0 g P25 $TiO_2$ powder and a certain amount of $Fe(NO_3)_3{\cdot}9H_2O$ were added into 50 ml deionized water, then the suspension was stirred for 1 h at the room temperature. The powder was collected and washed with deionized water for 3 times by centrifuging. Then the collected solid was dried at 100 °C for 24 h in the drying oven. The dry powder was then calcinated in a muffle furnace at 350 °C for 3 h. For comparison, the $Fe_2O_3/TiO_2$ composites with the different Ti/Fe atomic molar ratio were prepared using the above-mentioned method by adjusting the amount of $Fe(NO_3)_3{\cdot}H_2O$ to 0, 0.012, 0.025 and 0.05 g, which were marked $TiO_2$, FT0.125, FT0.25 and FT0.5, respectively. The preparation steps are shown in Fig. 1.

### 2.2. Materials characterizations

The crystalline structure of the photocatalysts was investigated by wide-angle X-ray diffractometer (XRD; Ultima IV 2036E102, Rigaku Corporation, Japan) with Cu Kα radiation at 50 Hz at the rate of 5 °C/min. The surface morphology and microstructure of the materials was measured by a field-emission scanning electron microscopy (SEM; SU8220, Hitachi, Japan). The adsorption of light was collected by UV–Vis spectra on a Perkin –Elmer Lambda 950 spectrometer (300–800 nm). Photoluminescence spectra (PL) of the samples was characterized by a Perkin–Elmer Luminescence spectrometer 55 (LS55). X-ray photoelectron spectra (XPS) was obtained on a spectrometer (Microlab 310 F Scanning Auger Microprobe, VG SCIENTIFIC LTD) with a constant pass energy of 50 eV by a monochromatic Al-Ka (1486.6 eV) X-ray. Electron spin resonance (ESR) signal of active radicals trapped by 5,5-dimethyl-1-pyrroline *N*-oxide (DMPO) was measured by a spectrometer (JES-FA200, JEOL, Japan) at 77 K. Fourier transform infrared spectroscopy (FTIR) spectra were recorded by a Thermofisher iN10 iZ10 infrared spectrophotometer.

### 2.3. Photocatalytic performance test

The photocatalytic performance of the sample was tested in a continuous flow reactor system. Herein, the gases used in the test were acetaldehyde and o-xylene. 4*65 W fluorescent lamps were used as light irradiation source, which were placed 20 cm above the photocatalysts. In order to be closer to the actual application, the temperature of the photocatalytic reaction was ambient temperature and the humidity in the chamber was the humidity in the air. 0.1 g as-prepared photocatalyst was coated on a 7.5 cm * 15 cm glass pane. Then this glass pane was put into the sealed reaction chamber with a transparent quartz cover and to reach an adsorption-desorption equilibrium under a continuous flow. After that, the fluorescent lamps were turn on. The removal ratio (η) of test gas was calculated through the following equation:

$$\eta = (1 - C/C_0) \times 100\%$$

where $C_0$ is the initial concentration and C is the concentration of test gas at different time intervals. The initial concentration values of acetaldehyde and o-xylene were 500 ppm and 50 ppm, respectively.

## 3. Results and discussion

### 3.1. Characterization of morphology and chemical composition

Fig. 2a and b shows the SEM image and EDS spectra of the sample FT0.25. There were aggregated $TiO_2$ nanoparticles in the vision and the size of $TiO_2$ nanoparticles was around 20–30 nm in diameter. Since by the impregnation method, a very low content of $Fe_2O_3$ was coupled with $TiO_2$. The EDS spectra showed that there were traces of Fe in the composites and proved the existence of $Fe_2O_3$. From the insert table it could be found that the weight percentage of Fe was 0.49% and the atomic percentage was only 0.19% for the FT0.25 sample.

XRD spectra was used to reveal the crystal structure of the samples. From Fig. 3a, the 2θ = 25.3°, 37.8°,48.0°, 54.0°, 54.9° and 62.8° are typical anatase peaks and 27.4°, 36.1°, 54.3° are typical rutile peaks. It was reported that by this impregnation method maghemite phase of γ-$Fe_2O_3$ was coupled with $TiO_2$ [32]. However, there were no additional peaks of $Fe_2O_3$ (typical peaks of γ-$Fe_2O_3$ appears at 2θ of 35.56° and 62.76°), since the low $Fe_2O_3$ content did not reach the detection limitation of XRD (no less than 5%). However, when magnify the peak

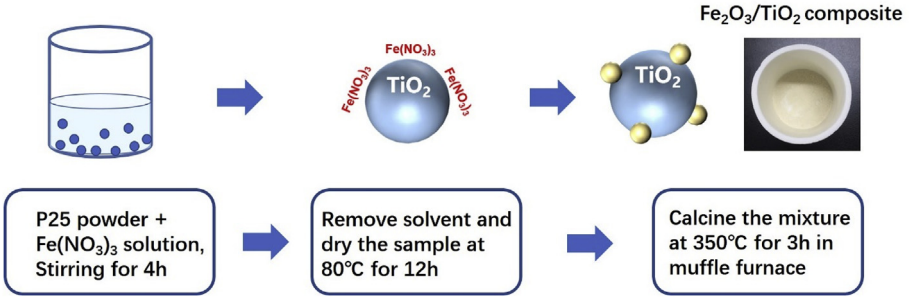


**Fig. 1.** The preparation steps of $Fe_2O_3/TiO_2$composites.

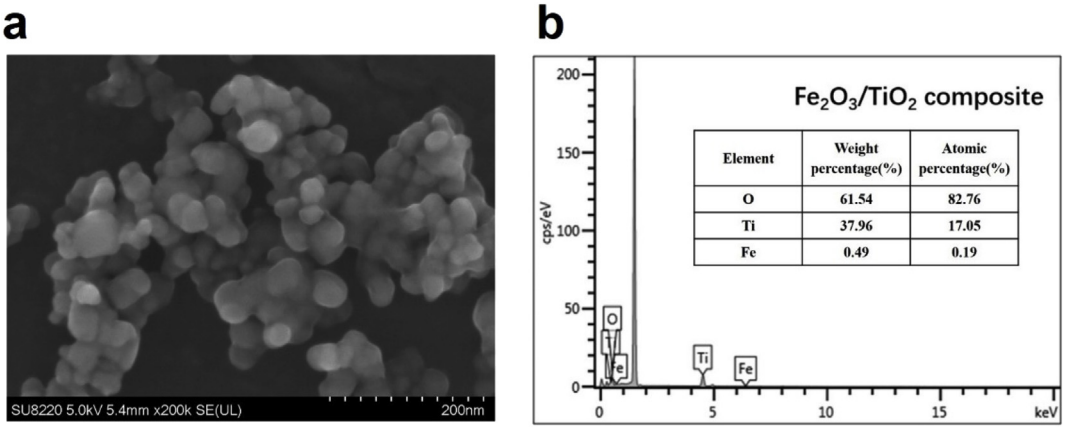


**Fig. 2.** (a) SEM and (b) EDS image of the sample FT0.25.

around 25.5°, it is clearly that the peak shifts to lower angle with the addition of $Fe_2O_3$, indicating that some lattice distortion occurred on the $TiO_2$ surface.

XPS spectra (Fig. 4a–d) was further used to confirm the presence of Fe, Ti and O elements. Fig. 4a shows Fe 2p1/2 (722.96 eV) and 2p3/2(709.69 eV). The weak peak of Fe2p proved the low content of $Fe_2O_3$, which was in line with the SEM image and XRD spectra. Ti 2p3/2 was around 458.32 eV and the Ti2p1/2 was around 464.18eV. The three peaks of O1s were ascribed to Ti-O bond, C=O bond and C-O bond respectively. Besides, there was C1s spectra (C-C, 284.8 eV; C-O, 286.5 eV; C=O, 288.5 eV) since the impurity of carbon was inevitable.

### 3.2. Photoelectrical properties of $Fe_2O_3/TiO_2$ composites

UV–vis absorption was used to detect the adsorption ability towards light of the samples. As illustrated in Fig. 5a, when coupling with $Fe_2O_3$, an improvement of UV–vis absorption were observed. To be specific, raw $TiO_2$ mainly adsorb light below 350 nm and had very weak adsorption in the visible range ($\lambda > 400$ nm). In contrast, the FT samples not only shows stronger adsorption of the light under 400 nm but also greatly prompt the visible light($400\text{ nm} < \lambda < 600\text{ nm}$). Since the band gap of $Fe_2O_3$ is about 2.3 eV [30], it can better make use of the visible light. Photoluminescence (PL) spectra (Fig. 5b) is an effective method of detecting the combination of photo-induced carriers. The pristine $TiO_2$ showed strong PL intensity since the photo-induced electrons and holes are easy to combine. When coupled with $Fe_2O_3$, the intensity of the PL decreased a lot. It could be explained by the structure of the composites. $Fe_2O_3$ and $TiO_2$ fabricated heterojunction and the built-in electric field were conductive to prevent electrons and holes from combing. Besides, $Fe_2O_3$ has lower conduction band and higher valence band than $TiO_2$, which means that the electrons of the $TiO_2$ can jump to the conduction band of $Fe_2O_3$ while the holes of the $TiO_2$ to the valence band of $Fe_2O_3$ [33].

### 3.3. Photocatalytic performance of $Fe_2O_3/TiO_2$ composites

After the properties detection, the photocatalytic performance of $Fe_2O_3/TiO_2$ composites towards two kinds of volatile organic compounds were further investigated. Acetaldehyde and o-xylene are typical aldehyde and benzenes. Although they both contains methyl ($-CH_3$), the function groups of acetaldehyde and o-xylene are formyl group (-CHO) and benzene ring ($-C_6H_5$), the mechanism of degradation should be different.

Fig. 6 shows that real-time $C/C_0$ after illumination. The initial concentration of acetaldehyde was 500 ppm and the flowing speed was 20 sccm. Clearly, all $Fe_2O_3/TiO_2$ composites showed higher photodegradation efficiency than pristine $TiO_2$ and FT0.25 attained the best photocatalytic performance. It means that when flowing through the surface of the photocatalyst, 80% of the acetaldehyde could be degraded by FT0.25. The initial concentration of o-xylene was 50 ppm and the flowing speed was 4 sccm. When reached a balance, the photodegradation efficiencies of pristine $TiO_2$, FT0.125, FT0.25 and FT0. 5 were 56%, 91%, 72% and 70% respectively (Table 1). $Fe_2O_3/TiO_2$ composites had better photocatalytic ability towards both acetaldehyde and o-xylene, since the composites can make better use of the visible light and promote the separation of photo-induced electrons and holes.

Notably, after 25 min, the $C/C_0$ increased after a decrease in the degradation of acetaldehyde while the $C/C_0$ of o-xylene kept stable

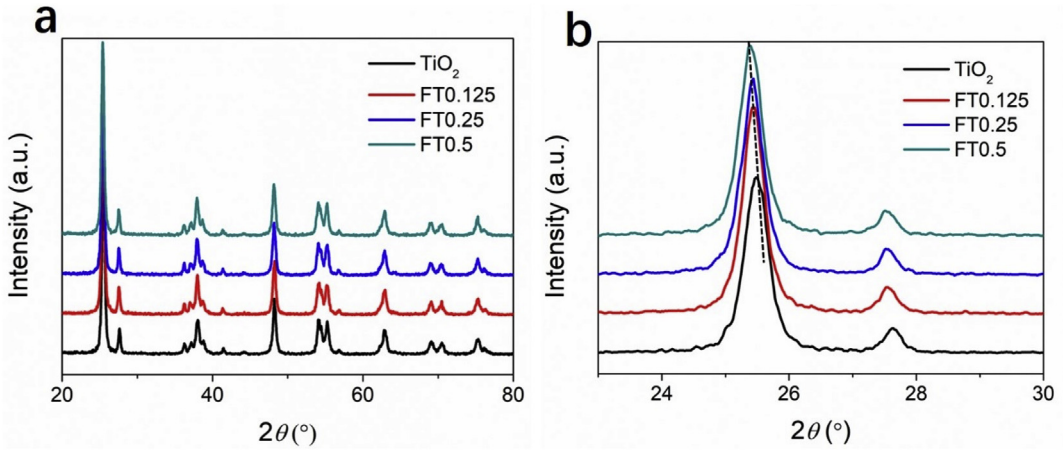


**Fig. 3.** (a) XRD spectra and (b) partial magnification spectra of $Fe_2O_3/TiO_2$ composites.

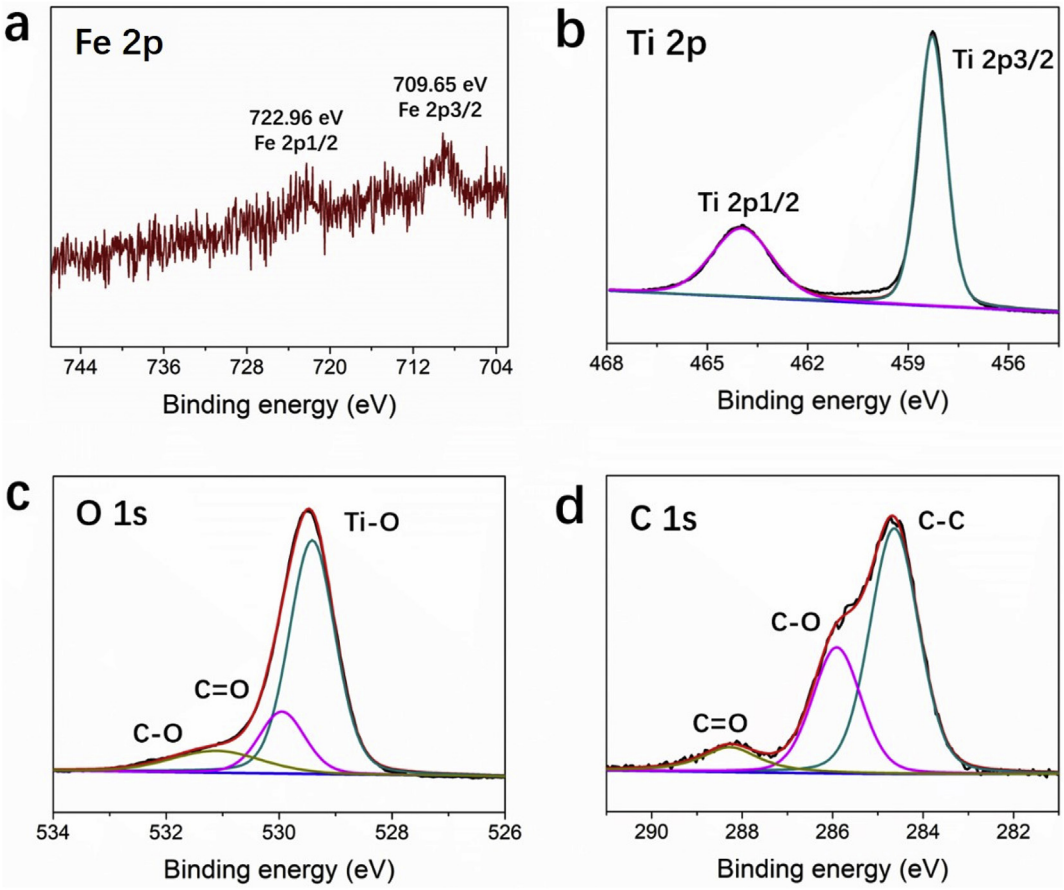


**Fig. 4.** XPS spectra of $Fe_2O_3/TiO_2$ composite.

even after 2 h. It was ascribed to the deactivation of the photocatalyst. After illumination, the photo-induced electrons transferred to $Fe_2O_3$ composite and $Fe^{3+}$ was reduced to $Fe^{2+}$ [34,35]. At the same time, acetaldehyde was oxidized to acetic acid. Since it is easy for $Fe^{2+}$ to combine with acetate (-COOH), $Fe_2O_3$ was gradually consumed and Fe $(CH_3OO)_2$ was produced. To further prove this assumption, the sample FT0.25 was put into muffle with 350 °C for 3 h and a recovery of the photocatalyst was found. $Fe(CH_3OO)_2$ can easily decompose under heat treatment in air and the final product is $Fe_2O_3$, thus it could be used for the regeneration of $Fe_2O_3/TiO_2$ photocatalyst. In contrast, o-xylene was oxidized into benzoic acid, which cannot react with $Fe^{2+}$ or $Fe^{3+}$. As a result the photocatalyst could stay stable. ESR was also used to prove the different reaction mechanism (Fig. 7). There are two peaks in the graph, g = 2 and g = 4.3 respectively, contributed by the $Fe_2O_3$. Since $Fe^{3+}$ was paramagnetic and can disturb the ESR signal, the peak at 324 mT (g = 2) of FT0.5 was broad [36,37]. After the degradation of acetaldehyde, the peak became sharp as a result of the consumption of $Fe^{3+}$. Meanwhile, the peak of FT0.5 had little change after degradation of o-xylene because the $Fe^{3+}$ could keep dynamic equilibrium in the photocatalytic process. The photodegradation curve and ESR signal corporately demonstrated that the deactivation of the $Fe_2O_3/TiO_2$ catalyst in the degradation of acetaldehyde was caused by the consumption of $Fe^{3+}$ and the production of $Fe(CH_3OO)_2$.

### 3.4. Mechanism of photocatalytic reaction

On the basis of the aforementioned properties and photodegradation performance investigation, a reasonable mechanism was proposed. As shown in scheme 1, when coupled with $Fe_2O_3$, the photo-induce electrons and holes on the $TiO_2$ can transfer to the $Fe_2O_3$ with lower

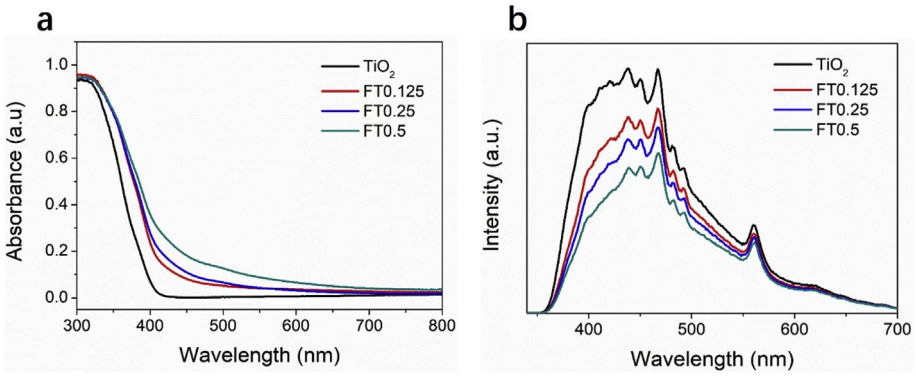


**Fig. 5.** (a) UV–Vis spectra and (b) Photoluminescence spectra of $Fe_2O_3/TiO_2$ composite.

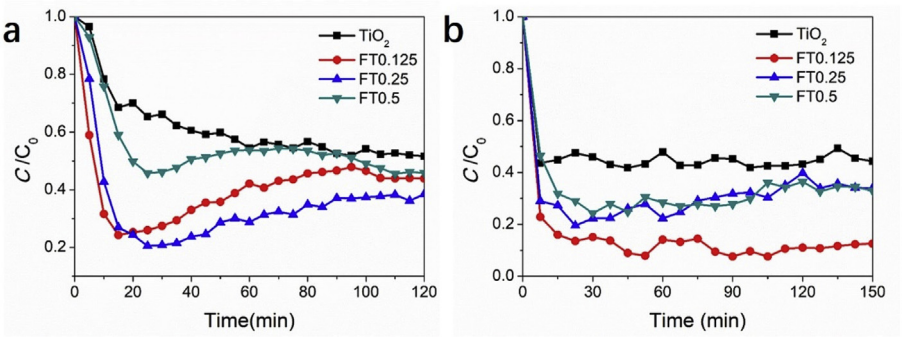


**Fig. 6.** Photodegradation of (a) acetaldehyde (500 ppm, 20 sccm) and (b) o-xylene (50 ppm, 4 sccm) under fluorescent lamp irradiation.

**Table 1**
Photodegradation efficiency of $TiO_2$ and $Fe_2O_3/TiO_2$ samples towards acetaldehyde and o-xylene.

| Sample | $TiO_2$ | FT0.125 | FT0.25 | FT0.5 |
|---|---|---|---|---|
| Acetaldehyde (500 ppm) | 48% | 78% | 80% | 55% |
| O-xylene (50 ppm) | 56% | 91% | 72% | 70% |

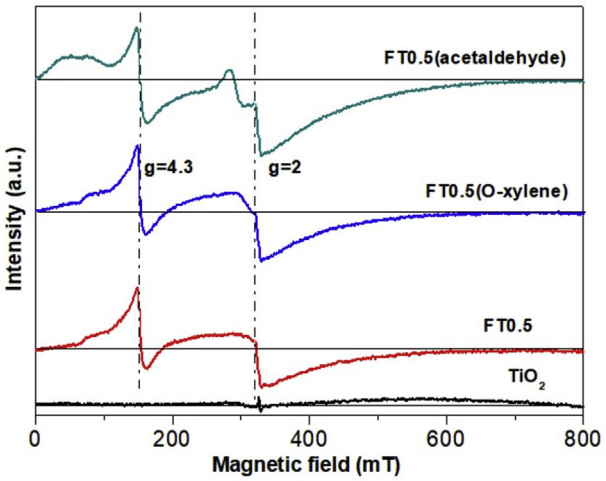


**Fig. 7.** ESR spectra of $Fe_2O_3/TiO_2$ composite before and after photocatalytic reaction towards acetaldehyde and o-xylene.

energy level, thus preventing the combination of them and promoting the photocatalytic ability of the catalysts. Besides, receiving the electrons, the $Fe^{3+}$ was reduced to $Fe^{2+}$. For the degradation of acetaldehyde, $CH_3CHO$ was first oxidized to $CH_3COOH$. Some acetate combined with $Fe^{2+}$ to produce $Fe(CH_3COO)_2$ and lead to the consumption of $Fe_2O_3$. As a result the photocatalytic efficiency of $Fe_2O_3/TiO_2$ composite decreased. The reaction equations are as follows:

$$TiO_2 + h\nu \rightarrow e^- + h^+ \quad (1)$$

$$e^- + O_2 \rightarrow \bullet O_2^- \quad (2)$$

$$h^+ + H_2O \rightarrow \cdot OH \quad (3)$$

$$Fe^{3+} + e^- \rightarrow Fe^{2+} \quad (4)$$

$$CH_3CHO + \cdot O_2^-/\cdot OH \rightarrow CH_3COOH \quad (5)$$

$$Fe^{2+} + CH_3COO^- \rightarrow Fe(CH_3COO)_2 \quad (6)$$

$$Fe(CH_3COO)_2 \xrightarrow{\Delta} Fe_2O_3 + CO_2 + H_2O \quad (7)$$

$$C_6H_5(CH_3)_2 + \cdot O_2^-/\cdot OH \rightarrow C_6H_5COOH \quad (8)$$

$$C_6H_5COOH + \cdot O_2^-/\cdot OH + Fe^{2+} \rightarrow \ldots \rightarrow Fe^{3+} + CO_2 + H_2O \quad (9)$$

In contrast, the intermediate product of o-xylene was benzoic acid [38,39], which could not combine with $Fe^{3+}$ or $Fe^{2+}$, so the photocatalytic reaction could keep stable.

## 4. Conclusions

In this work, $Fe_2O_3/TiO_2$ composites were fabricated by the impregnation method. By coupling with $Fe_2O_3$, the adsorption of visible light was promoted and the combination of electrons and holes was prevented, thus the photodegradation efficiency of the composites was improved a lot. In the degradation of acetaldehyde and o-xylene, all $Fe_2O_3/TiO_2$ composites showed better photocatalytic efficiency than pristine $TiO_2$. Notably, the deactivation of the $Fe_2O_3/TiO_2$ catalysts occurred in acetaldehyde degradation process after 25 min while there was no such phenomenon in the degradation of o-xylene. It was ascribed to that acetaldehyde was oxidized to acetic acid and combined with the produced $Fe^{2+}$, which caused the consumption of $Fe_2O_3$. In contrast, the intermediate product of o-xylene did not react with $Fe^{2+}$ or $Fe^{3+}$, thus the photocatalyst could keep dynamic stable. ESR signal was further used to demonstrate the process of the photocatalytic reaction. This work not only provide a feasible method of improving the photocatalytic ability of the catalyst, but also help us deeply understand

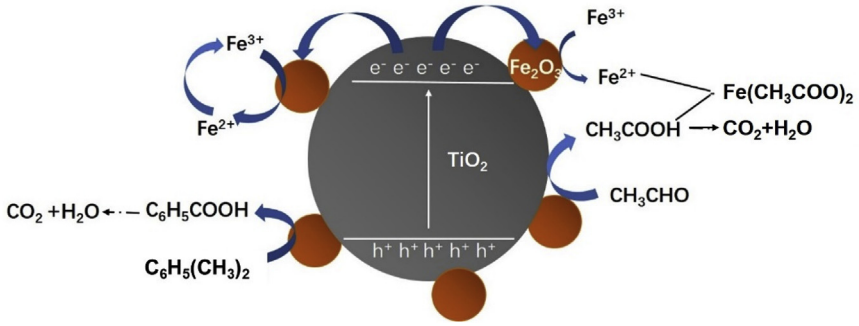


**Scheme 1.** Schematic structure of the $Fe_2O_3/TiO_2$ composite and the main process of photodegradation for acetaldehyde and o-xylene.

the process of the photodegradation.

## Conflicts of interest

There are no conflicts to declare.

## Acknowledgement

This work was financially supported by the National Key Research and Development Program of China (2016YFA0203000), the NSFC-DFG bilateral organization program (51761135107) and Shanghai Sailing Program (18YF1426800).

## References

[1] A.J. Jafari, R.R. Kalantary, A. Esrafili, H. Arfaeinia, Synthesis of silica-functionalized graphene oxide/ZnO coated on fiberglass and its application in photocatalytic removal of gaseous benzene, Process Saf. Environ. Protect. 116 (2018) 377–387.
[2] L. Yu, L. Wang, W. Xu, L. Chen, M. Fu, J. Wu, D. Ye, Adsorption of VOCs on reduced graphene oxide, J. Environ. Sci. (China) 67 (2018) 171–178.
[3] H.K. MA, W.C. Morris, M. Galloway, A.S. BM, C.J. Percival, D.E. Shallcross, An estimation of the levels of stabilized criegee intermediates in the UK urban and rural atmosphere using the steady-state approximation and the potential effects of these intermediates on tropospheric oxidation cycles, Int. J. Chem. Kinet. 49 (2017) 611–621.
[4] G. Pecchi, P. Reyes, R. Zamora, L.E. Cadús, J.L.G. Fierro, Surface properties and performance for VOCs combustion of LaFe1 − yNiyO3 perovskite oxides, J. Solid State Chem. 181 (2008) 905–912.
[5] S.J. Lue, W.W. Chen, S.Y. Wu, L.D. Wang, C.H. Kuo, Vapor permeation modeling of multi-component systems using a poly(dimethylsiloxane) membrane, J. Membr. Sci. 311 (2008) 380–389.
[6] E.N.S.A.V. Vorontsov, G.B. Barannik, V.N. Troitsky, V.N. Parmon, Quantitative studies on the heterogeneous gas-phase photooxidation of CO and simple VOCs by air over TiO2, Catal. Today 39 (1997) 207–218.
[7] S. Sun, W. Wang, L. Zhang, Efficient contaminant removal by Bi2WO6 films with nanoleaflike structures through a photoelectrocatalytic process, J. Phys. Chem. C 116 (2012) 19413–19418.
[8] I. Cimieri, H. Poelman, N. Avci, J. Geens, S.D. Lambert, B. Heinrichs, D. Poelman, Sol–gel preparation of pure and doped TiO2 films for the photocatalytic oxidation of ethanol in air, J. Sol. Gel Sci. Technol. 63 (2012) 526–536.
[9] Y.-z. Qu, M.-m. Yao, F. Li, X.-h. Sun, Microstructures and photocatalytic properties of Fe3 + /Ce3 + codoped nanocrystalline TiO2 films, Water, Air, & Soil Pollution 221 (2011) 13–21.
[10] D. Wang, T. Kako, J. Ye, Efficient photocatalytic decomposition of acetaldehyde over a solid-solution perovskite (Ag0.75Sr0.25)(Nb0.75Ti0.25)O3 under visible-light irradiation, J. Am. Chem. Soc. 130 (2008) 2724–2725.
[11] T. Ochiai, A. Fujishima, Photoelectrochemical properties of TiO2 photocatalyst and its applications for environmental purification, J. Photochem. Photobiol. C Photochem. Rev. 13 (2012) 247–262.
[12] M. Pelaez, P. Falaras, V. Likodimos, A.G. Kontos, A.A. de la Cruz, K. O'Shea, D.D. Dionysiou, Synthesis, structural characterization and evaluation of sol–gel-based NF-TiO2 films with visible light-photoactivation for the removal of microcystin-LR☆, Appl. Catal. B Environ. 99 (2010) 378–387.
[13] X. Tang, Q. Feng, K. Liu, X. Luo, J. Huang, Z. Li, A simple and innovative route to remarkably enhance the photocatalytic performance of TiO 2 : using micro-meso porous silica nanofibers as carrier to support highly-dispersed TiO 2 nanoparticles, Microporous Mesoporous Mater. 258 (2018) 251–261.
[14] X. Liu, L. Pan, T. Lv, Z. Sun, C.Q. Sun, Visible light photocatalytic degradation of dyes by bismuth oxide-reduced graphene oxide composites prepared via microwave-assisted method, J. Colloid Interface Sci. 408 (2013) 145–150.
[15] M.R. Bayati, F. Golestani-Fard, A.Z. Moshfegh, R. Molaei, A photocatalytic approach in micro arc oxidation of WO3–TiO2 nano porous semiconductors under pulse current, Mater. Chem. Phys. 128 (2011) 427–432.
[16] D. Wang, L. Xiao, Q. Luo, X. Li, J. An, Y. Duan, Highly efficient visible light TiO2 photocatalyst prepared by sol-gel method at temperatures lower than 300 degrees C, J. Hazard Mater. 192 (2011) 150–159.
[17] Y. Takahashi, T. Tatsuma, Visible light-induced photocatalysts with reductive energy storage abilities, Electrochem. Commun. 10 (2008) 1404–1407.
[18] Y. Geng, H. Huang, X. Chen, H. Ding, S. Yang, F. Liu, W. Shan, The effect of Ce on a high-efficiency CeO2/WO3–TiO2 catalyst for the selective catalytic reduction of NOx with NH3, RSC Adv. 6 (2016) 64803–64810.
[19] Q. Wang, Z. Liu, R. Jin, Y. Wang, S. Gao, SILAR preparation of Bi2S3 nanoparticles sensitized TiO2 nanotube arrays for efficient solar cells and photocatalysts, Separ. Purif. Technol. 210 (2019) 798–803.
[20] X. Yan, K. Ye, T. Zhang, C. Xue, D. Zhang, C. Ma, J. Wei, G. Yang, Formation of three-dimensionally ordered macroporous TiO2@nanosheet SnS2 heterojunctions for exceptional visible-light driven photocatalytic activity, New J. Chem. 41 (2017) 8482–8489.
[21] W.-K. Jo, T. Adinaveen, J.J. Vijaya, N.C. Sagaya Selvam, Synthesis of MoS2 nanosheet supported Z-scheme TiO2/g-C3N4 photocatalysts for the enhanced photocatalytic degradation of organic water pollutants, RSC Adv. 6 (2016) 10487–10497.
[22] M. Nasirian, M. Mehrvar, Photocatalytic degradation of aqueous methyl orange using a novel Ag/TiO2/Fe2O3 photocatalyst prepared by UV-assisted thermal synthesis, Desalination and Water Treatment 137 (2019) 371–380.
[23] L. Sun, W. Wu, Q. Tian, M. Lei, Z. Dai, X. Xiao, F. Ren, C. Jiang, Carbon and silica interlayer influence for the photocatalytic performances of spindle-like α-Fe 2 O 3/Bi 2 O 3 p – n heterostructures, Mater. Sci. Semicond. Process. 41 (2016) 411–419.
[24] J. Zeng, J. Li, J. Zhong, H. Yang, Y. Lu, G. Wang, Improved Sun light photocatalytic activity of α-Fe 2 O 3 prepared with the assistance of CTAB, Mater. Lett. 160 (2015) 526–528.
[25] A. Banisharif, A.A. Khodadadi, Y. Mortazavi, A. Anaraki Firooz, J. Beheshtian, S. Agah, S. Menbari, Highly active Fe 2 O 3 -doped TiO 2 photocatalyst for degradation of trichloroethylene in air under UV and visible light irradiation: experimental and computational studies, Appl. Catal. B Environ. 165 (2015) 209–221.
[26] A. Amarjargal, Z. Jiang, L.D. Tijing, C.-H. Park, I.-T. Im, C.S. Kim, Nanosheet-based α-Fe2O3 hierarchical structure decorated with TiO2 nanospheres via a simple one-pot route: magnetically recyclable photocatalysts, J. Alloy. Comp. 580 (2013) 143–147.
[27] H. Tang, D. Zhang, G. Tang, X. Ji, W. Li, C. Li, X. Yang, Hydrothermal synthesis and visible-light photocatalytic activity of α-Fe2O3/TiO2 composite hollow microspheres, Ceram. Int. 39 (2013) 8633–8640.
[28] J. Huang, O. Buyukcakir, M.W. Mara, A. Coskun, N.M. Dimitrijevic, G. Barin, O. Kokhan, A.B. Stickrath, R. Ruppert, D.M. Tiede, J.F. Stoddart, J.-P. Sauvage, L.X. Chen, Highly efficient ultrafast electron injection from the singlet MLCT excited state of copper(I) diimine complexes to TiO2 nanoparticles, Angew. Chem. Int. Ed. 51 (2012) 12711–12715.
[29] J.B. Priebe, M. Karnahl, H. Junge, M. Beller, D. Hollmann, A. Brueckner, Water reduction with visible light: synergy between optical transitions and electron transfer in Au-TiO2 catalysts visualized by in situ EPR spectroscopy, Angew. Chem. Int. Ed. 52 (2013) 11420–11424.
[30] W.-H. Hung, T.-M. Chien, C.-M. Tseng, Enhanced photocatalytic water splitting by plasmonic TiO2-Fe2O3 cocatalyst under visible light irradiation, J. Phys. Chem. C 118 (2014) 12676–12681.
[31] P. Luan, M. Xie, D. Liu, X. Fu, L. Jing, Effective charge separation in the rutile TiO2 nanorod-coupled alpha-Fe2O3 with exceptionally high visible activities, Sci. Rep. 4 (2014).
[32] S.R. Mirmasoomi, M.M. Ghazi, M. Galedari, Photocatalytic degradation of diazinon under visible light using TiO2/Fe2O3 nanocomposite synthesized by ultrasonic-assisted impregnation method, Separ. Purif. Technol. 175 (2017) 418–427.
[33] H. Liu, Z.-G. Zhang, X.-X. Wang, G.-D. Nie, J. Zhang, S.-X. Zhang, N. Cao, S.-Y. Yan, Y.-Z. Long, Highly flexible Fe2O3/TiO2 composite nanofibers for photocatalysis and ultraviolet detection, J. Phys. Chem. Solids 121 (2018) 236–246.
[34] C. Guo, R. Zhang, B. Wang, Y. Qu, Visible-light-driven Fe2O3 nanoparticles/TiO2 array photoelectrode and its photoelectrochemical property, Res. Chem. Intermed. 42 (2016) 7935–7946.
[35] H. Zhao, W. Fu, H. Yang, Y. Xu, W. Zhao, Y. Zhang, H. Chen, Q. Jing, X. Qi, J. Cao, X. Zhou, Y. Li, Synthesis and characterization of TiO2/Fe2O3 core-shell nanocomposition film and their photoelectrochemical property, Appl. Surf. Sci. 257 (2011) 8778–8783.
[36] E. Antoni, L. Montagne, S. Daviero, G. Palavit, J.L. Bernard, A. Wattiaux, H. Vezin, Structural characterization of iron-alumino-silicate glasses, J. Non-Cryst. Solids 345 (2004) 66–69.
[37] E.S. Dunaeva, E.A. Ugolkova, N.N. Efimov, V.V. Minin, V.M. Novotortsev, ESR spectroscopy of FeIII ions in sodium silicate glasses, Russ. Chem. Bull. 63 (2014) 60–63.
[38] C.C. Pei, W.W.-F. Leung, Photocatalytic oxidation of nitrogen monoxide and o-xylene by TiO2/ZnO/Bi2O3 nanofibers: optimization, kinetic modeling and mechanisms, Appl. Catal. B Environ. 174 (2015) 515–525.
[39] W. Lin, X. Xie, X. Wang, Y. Wang, D. Segets, J. Sun, Efficient adsorption and sustainable degradation of gaseous acetaldehyde and o-xylene using rGO-TiO 2 photocatalyst, Chem. Eng. J. 349 (2018) 708–718.